tvst

Cornea & External Disease

A Method for Visualizing Corneal Dynamics Through Pixel Intensity Tracking

Ana R. Arizcuren[1] **and Alejandra Consejo**[1]

[1] Aragon Institute for Engineering Research (I3A), University of Zaragoza, Zaragoza, Spain

Correspondence: Ana R. Arizcuren, Aragon Institute for Engineering Research (I3A), University of Zaragoza, C/ María de Luna 3, Zaragoza 50018, Spain. e-mail: ana.arizcuren@unizar.es

Received: August 5, 2024
Accepted: May 1, 2025
Published: June 12, 2025

Keywords: corneal biomechanics; Corvis ST; HSV color space; aging; image processing

Citation: Arizcuren AR, Consejo A. A method for visualizing corneal dynamics through pixel intensity tracking. Transl Vis Sci Technol. 2025;14(6):24, https://doi.org/10.1167/tvst.14.6.24

Purpose: To develop a methodology for analyzing dynamic corneal images using pixel intensity tracking and hue, saturation, and value (HSV) color space transformation, aiming to quantify and visually interpret corneal responsiveness to mechanical stimulation.

Methods: This study utilized the OCULUS Corvis ST device to obtain dynamic corneal images from two subject groups (young and older individuals). To ensure accurate pixel tracking, segmentation and registration techniques were implemented. To counteract potential biases due to alterations in curvature and eye retraction caused by the air-puff mechanical stimulus, the last 30 frames available post-stimulus were used for analysis. Pixel intensity tracking calculations were then performed in the frequency domain to compute H, S, and V values for each pixel within the overall region of interest. Additionally, corneal biomechanical parameters from the Corvis ST were extracted to examine their relationship with HSV values.

Results: The HSV transformation provided a quantitative visual interpretation of corneal dynamics, with reddish vibrant areas indicating higher responsiveness to mechanical stimulation and dull blue areas indicating lower responsiveness. Additionally, significant differences were found between the young and older groups in each of the three HSV channels (all $P < 0.001$). Four biomechanical parameters showed statistically significant differences between groups ($P < 0.05$), but no statistically significant correlation with HSV values was found.

Conclusions: The HSV methodology effectively visualizes and quantifies corneal responsiveness to mechanical stimulation, offering a new approach for assessing corneal dynamics.

Translational Relevance: HSV color space analysis has the potential to enhance the diagnosis and management of conditions in which corneal dynamics are affected.

Introduction

Air-puff corneal deformation is a widely used clinical technique in intraocular pressure assessments. Among the available clinical devices, the Corvis ST (OCULUS Optikgeräte GmbH, Wetzlar, Germany) is unique in its ability to capture dynamic corneal images during air-puff stimulation using a high-speed Scheimpflug camera. The ability to record images during an air-puff stimulus is crucial for characterizing various aspects of the corneal response to mechanical stimuli, such as displacement and applanation. This capability enables a comprehensive analysis of the evolution of the corneal shape in response to the stimulus, an aspect crucial for the study of corneal biomechanics.[1] Through the examination of these deformation patterns, clinicians and researchers gain essential insights into the structural integrity[2] and overall health[3] of the cornea.

Despite these advancements, key biomechanical properties such as stiffness, elasticity, and viscoelasticity are not directly measurable in vivo using clinical devices. As a result, researchers and clinicians must rely on surrogate parameters derived from Corvis ST measurements to infer corneal biomechanical behavior. Although these parameters have proven useful in distinguishing between healthy and pathological

corneas,[4] they often fail to differentiate between groups when tissue changes are more subtle.[5] For example, corneal tissue is known to change with age,[6–8] and multiple studies have attempted to differentiate younger from older individuals using standard Corvis ST parameters. However, results have been inconsistent, and no consensus has been reached on which Corvis ST biomechanical metrics reliably capture age-related changes in corneal tissue.[6–8]

To extend biomechanical analysis beyond built-in Corvis ST parameters, researchers have explored exporting Corvis ST image sequences to conduct custom evaluations of corneal deformation. These studies have primarily focused on the anterior corneal border, analyzing parameters such as corneal curvature changes, displacement, applanation, and eye rotation as a consequence of air-puff deformation.[9,10] Although these approaches provide valuable insights, they focus exclusively on the outermost corneal surface and fail to capture the response of deeper corneal layers.

The present study introduces a fundamentally distinct strategy for assessing corneal responsiveness to mechanical stimulation. Drawing inspiration from the pioneering efforts of Scholler et al.,[11] who employed full-field optical coherence tomography (FF-OCT) for the dynamic visualization of retinal organoids, the current work adopts an equivalent pixel-intensity tracking analytical approach. Scholler's methodology, which hinges on tracking and individually examining the temporal evolution of each pixel intensity, facilitates a transition from grayscale imaging to a more informative color representation, specifically to the hue, saturation, and value (HSV) color space. In their methodology, dynamic analysis of pixel intensity enables each HSV channel to represent an independent physical property, with each channel carrying distinct information that could serve as a biomarker for tissue characterization. As a result, one can readily discern which regions of an image exhibit higher responsiveness to motion relative to others. This study aimed to implement pixel intensity tracking analysis on clinically obtained dynamic corneal images. By applying this methodology, corneal responsiveness is associated with color representation, enabling a quantitative visual interpretation of corneal dynamics.

Methodology

Data Collection

This study includes retrospective data obtained from the Corvis ST air-puff tonometer. Two groups of Caucasian subjects were considered: a group of 38 young subjects of age ≤30 years (24 ± 2 years old; range, 20–30 years; 66% women and 34% men) and a group of 35 older subjects of age ≥47 years (58 ± 6 years old; range, 47–73 years; 74% women and 26% men). Only one eye was considered per subject. This group choice aimed to create two subject cohorts with contrasting corneal tissue properties, given the well-established influence of age on corneal tissue.[6] Subjects with a history of ocular or corneal surgery, any eye disease or systemic condition known to affect ocular health, or long-term use of topical medications were excluded from the study.

Data Preprocessing

For each subject, Corvis ST data included a sequence of 140 Scheimpflug images captured every 230 µs showing the corneal dynamic response to an air-puff stimulus (Fig. 1). To ensure pixel tracking consistency in our analysis, the last 30 frames from each sequence were considered (Fig. 1). This selection was guided by the objective of maximizing the available temporal data points, circumventing the issue of corneal curvature changes occurring during air-puff deformation.[10] By limiting the analysis to these 30 frames, we focused on a segment of the data unaffected by the curvature changes,[10] thereby maintaining the integrity of the pixel tracking process. The grayscale original images were sized at 576 × 200 pixels (Fig. 2a.1). The fixed region of interest (ROI) within each frame was defined as a specific area on the corneal periphery, situated 2.5 mm right of the corneal apex and 1.2 mm from the top edge of the image. This positioning ensured that the cornea was always fully contained within the ROI without any unwanted cuts, as depicted in Figure 2a.2. The corneal apex was determined by identifying the highest point on the cornea in the first frame of the selected 30-frame sequence. The ROI maintained consistent dimensions of 107 × 131 pixels in each frame, approximately corresponding to 1.5 × 3 mm, based on the image resolution of the instrument.[12] The strategic selection of the peripheral cornea instead of the central region was driven by an intention to replicate the conditions of milder corneal stimuli in our analysis. This methodological preference further minimizes potential artifacts associated with tracking each individual pixel over time (Fig. 2a.3).

After ROI selection, each frame had the cornea segmented and registered. The first was necessary to separate corneal pixels from the background, and the latter was essential to ensure a repeatable pixel position. Corneal segmentation was achieved by identifying the anterior and posterior corneal boundaries using traditional image processing techniques, includ-

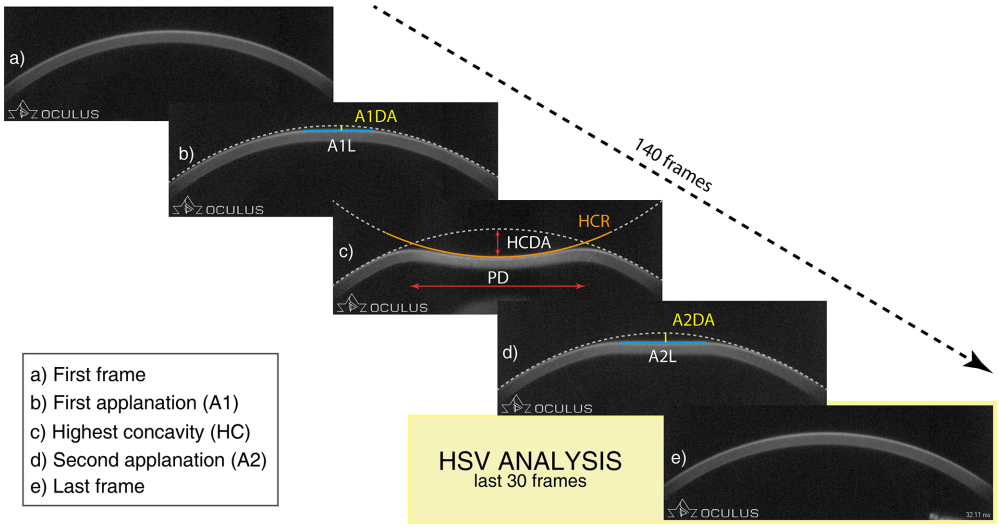

Figure 1. Selected frames from the 140-frame sequence provided by the Corvis ST for biomechanical analysis of the cornea. (**a**) First frame of the sequence, corresponding to the initial corneal configuration prior to the application of the air puff. The selected frames illustrate key deformation stages, including first applanation, A1 (**b**); highest concavity, HC (**c**); and second applanation, A2 (**d**). Additionally, some key parameters from the built-in proprietary software are illustrated. The highlighted region (HSV analysis) represents the last 30 frames used for the HSV analysis in the current work. A1DA, deformation amplitude at A1; A1L, length of the flattened segment; A2DA, deformation amplitude at A2; A2L, length of the flattened segment; HCDA, distance of the corneal apex movement from the initiation of the deformation to HC; PD, distance between the two surrounding peaks of the cornea at HC; HCR, central curvature radius at HC.

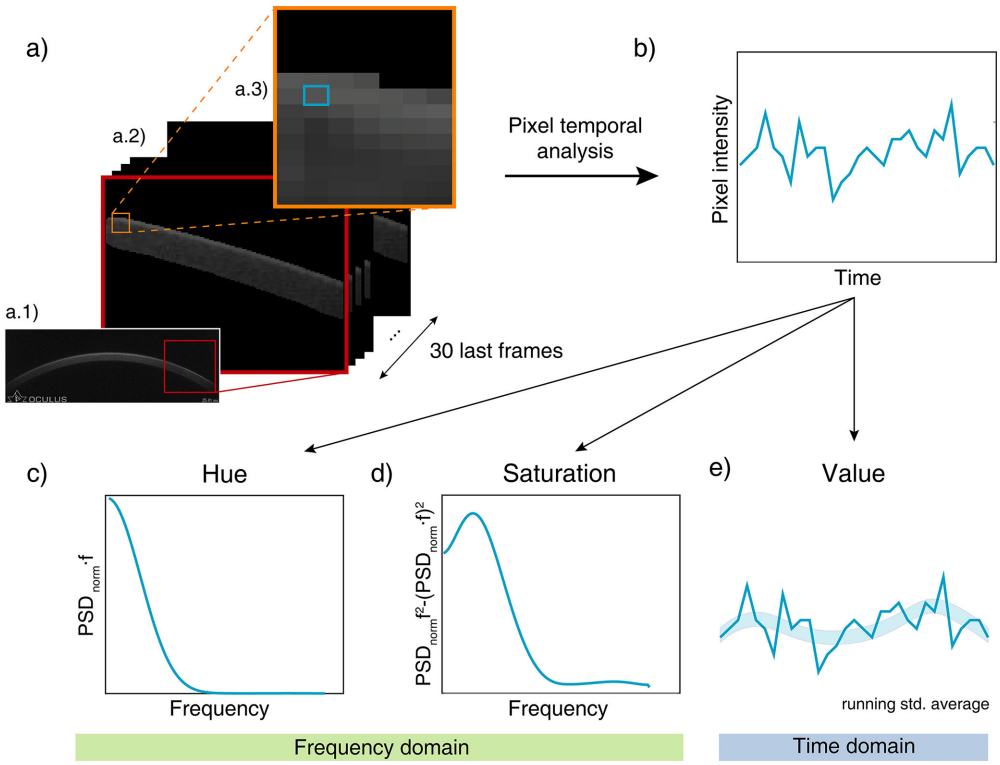

Figure 2. Main steps to obtain the three channels necessary for HSV image representation. From the original Corvis ST images (**a.1**), only the last 30 frames were analyzed, considering the peripheral corneal as the ROI (**a.2**). Each individual pixel from the ROI (an exemplary pixel marked in blue in **a.3**) was further analyzed across the selected 30 frames. Hence, pixel intensity variations per pixel over time were evaluated (**b**). From signal (**b**), the power spectrum density (PSD) was evaluated and used, along with frequency *f*, to compute the hue (**c**) and the saturation (**d**). Value was calculated as the average of the running standard deviation of the mean pixel intensity over time (**e**). The process (**b**–**e**) was repeated for each pixel from the ROI (**a.2**).

ing median filtering and edge detection, as detailed in prior studies.[13] The initial frame served as a reference to maintain a uniform number of pixels within the ROI. This process involved identifying both anterior and posterior borders exclusively in the first frame. In corneal segmentation with the Corvis ST, the anterior border identification is often more straightforward and reliable compared to defining the posterior border, due to factors such as image contrast and anterior eye biometry. Consequently, for the subsequent 29 frames, only the anterior border was detected, and the posterior border was inferred based on the corneal thickness determined from the first frame. The corneal thickness was calculated by measuring the distance between the anterior and posterior borders specifically in the ROI of the cornea. This methodology guaranteed a consistent pixel count across all frames, thereby ensuring pixel uniformity in the analysis. Additionally, registration had to be considered because the air-puff stimulus applied to the center of the cornea indirectly induces eye retraction, especially during stimulation.[9] Although our analysis considered the last 30 post-air-puff frames, we used registration to assess corneal displacement during mechanical recovery. A rigid-body registration was performed by taking the segmented anterior corneal profile in the first frame as a reference, measuring its distance from the top edge of the image and aligning all frames accordingly to maintain a consistent vertical position. This approach ensured repeatable pixel positioning across frames. Corneal displacement and eye retraction are interchangeable terms previously used in related literature. The accuracy of both the segmentation and registration processes was evaluated using the Dice coefficient, which ranges from 0 to 1, where 1 indicates perfect overlap and 0 denotes no overlap. The Dice coefficient was calculated individually for each subject, yielding a mean value of 0.98 ± 0.01, confirming the high precision and consistency of the method across frames.

Corneal Excitation

The Corvis ST air puff is well characterized in the literature.[14–17] In the Corvis ST, a transient load type is applied to the cornea. The air-puff pressure stimulus has the following functional form[15]:

$$p(t, r) = p_0 \exp\left[-64\left(\frac{t}{T} - \frac{1}{4}\right)^2\right] \exp\left(-0.44r^2\right) \quad (1)$$

where p_0 is the maximum magnitude of the air-puff pressure (13 kPa),[15,16] $T/2$ is the duration of the air puff (20 ms),[15] and r is the distance from the nozzle to a point on the corneal surface apex (11 mm).[15] In the current study, given the consideration of the peripheral cornea, a radial correction was necessary to estimate the magnitude of the corneal stimulus. As per Eliasy et al.,[16] a correction equivalent to 15% of the maximum pressure is recommended for a corneal position 2.5 mm away from the corneal apex. Taking these factors into account, it is estimated that the stimulus exerted on an area under examination is approximately 0.5 kPa.

HSV Analysis

The HSV color space is a color representation model that aligns more intuitively with human perception of color, contrasting with the conventional red, green, blue (RGB) system, which is based on additive primaries. Hue represents the color itself, defined as a position on a circular color wheel ranging from 0° to 360°. In this standard representation, 0° and 360° correspond to red, 120° to green, and 240° to blue. Saturation measures the intensity or purity of a color. At 0%, the color lacks intensity and appears desaturated or dull, whereas at 100% the color is vivid and fully saturated. Value, or brightness, adjusts the lightness or darkness of a color, spanning from complete darkness (0%) to full brightness (100%), effectively modifying the illumination of the color without altering its actual hue. This structure of color definition and manipulation in the HSV model allows for a more intuitive handling of color, closely resembling how humans perceive and interact with the spectrum of colors in the natural world.[18]

On the other hand, the grayscale color space does not use color information; it only records brightness. The images in grayscale color space, as captured by the ophthalmic device, contain a single channel with values ranging from pure black (at the weakest intensity, value 0) to pure white (at the strongest intensity, value 255) (Fig. 2a). Grayscale is strictly about the intensity of light, not the quality of the color itself. However, Scholler et al.[11] converted dynamic OCT grayscale images to HSV color space images, linking the channels to frequencies related to responsiveness to mechanical stimulation. Scholler and colleagues suggested that, in the HSV color space, the brightness of an image correlates with the amplitude of fluctuations, and the color relates to the speed of these fluctuations, from blue (slow) to red (fast) through green (in between).[11] Their approach where images are processed in the HSV color space differs from the RGB color space because it allows each of the three channels to represent a specific physical property, enhancing quantita-

tive visual interpretation.[11] The idea is to attribute a color for each pixel depending on the characteristic time period or frequency of the dynamic signal considering each individual pixel as a sum of random walks.[11]

Following the methodology of Scholler et al.,[11] the first step was to use the dynamic intensity variation per pixel (Fig. 2b) to compute the power spectrum density (PSD) using Welch's method for each pixel and then use an L1 normalization on each PSD as if it were a probability distribution. Then, the hue channel was computed as the mean frequency:

$$\mathrm{H} = <f> = PSD_{norm} \cdot f \tag{2}$$

where PSD_{norm} is the normalized PSD array, f is the frequency, and "·" is the dot product (Fig. 2c). The H values were strategically inverted, ensuring a more intuitive interpretation where red indicates rapid movement and blue denotes slowness. Additionally, the H values were rescaled to fall between 0 and 0.66. This adjustment is crucial, as the hue in the HSV color space is depicted as a wheel where values of 0 and 1 (i.e., 0° and 360°) correspond to the same color, red. Thus, this adjustment avoids redundancy in color representation and aids in the clear, intuitive differentiation of movement speeds in the final HSV image. Further, saturation was computed as the inverse of the normalized PSD bandwidth. As a consequence, the saturation channel carries the frequency bandwidth information. In practice, it is computed as the standard deviation of the frequencies (i.e., it corresponds to the frequency histogram width) as:

$$S = \sqrt{PSD_{norm} \cdot f^2 - (PSD_{norm} \cdot f)^2} \tag{3}$$

where PSD_{norm} is the normalized PSD array, f is the frequency, and "·" is the dot product (Fig. 2d): the wider the spectrum, the lower the saturation. White noise has a broader bandwidth and will, therefore, appear grayish instead of colored. To obtain a single value per pixel of H and S, the area under the curve of the resulting curve (Figs. 2c and 2d, respectively) was calculated and rescaled. Finally, the value (which corresponds to the perceived pixel intensity) was computed as the average of the running standard deviation of the mean pixel intensity over time with a window size set at 10% of the samples, in accordance with Scholler et al.[11] (Fig. 2e). After computing the three channels, the dynamic image was transformed into the RGB color space for display purposes.

Corneal Biomechanics Parameters

In addition to HSV analysis, we investigated whether H, S, and V parameters carry complementary or correlated information relative to the proprietary biomechanical parameters of the Corvis ST. To gain a comprehensive understanding of corneal behavior, 19 biomechanical parameters were analyzed and categorized into three distinct phases: first applanation (A1), second applanation (A2), and highest concavity (HC) (Fig. 1). These parameters were obtained from a sequence of 140 frames recorded during the corneal deformation process, capturing its biomechanical response over time (Fig. 1).

The extracted biomechanical parameters, obtained directly from the Corvis ST software, include time from the start to each applanation event (A1T, A2T), length of the flattened segment (A1L, A2L), velocity of the corneal apex at applanation (A1V, A2V), deformation amplitude (A1DA, A2DA), deflection (A1DefA, A2DefA), deflection area (A1DefArea, A2DefArea), and arc length change (A1dArcL, A2dArcL), as well as additional parameters such as corneal apex movement distance (HCDA), peak distance (PD), and central curvature radius at HC (HCR).

Statistical Analysis

In addition to computing the HSV image, the mean values of the H, S, and V channels for each subject were computed. To determine whether significant differences existed between younger and older subjects in the H, S, and V values, we conducted a univariate analysis of variance (ANOVA), treating the measured eye (right/left) as a random factor. Shapiro–Wilk test, Mauchly's test of sphericity, and Levene's test indicated that the assumptions of normality, sphericity, and homogeneity of variances, respectively, had not been violated. The level of significance was established at 0.05. The random factor did not interact with the other variables; therefore, the right and left eyes were treated as indistinguishable. Additionally, to compare our findings against those from existing literature investigating corneal vibrations with the Corvis ST, we executed an independent t-test on corneal displacement, comparing the two study groups. Corneal displacement quantification is necessary for accurate corneal registration. Further, we calculated and compared the group mean corneal frequencies obtained for the epithelium (considered as the 10% of corneal thickness[20]) with those from the stroma, considered as the remaining corneal thickness.

For the analysis of corneal biomechanical parameters, an independent t-test was performed to assess differences between age groups. Additionally, these parameters were correlated with H, S, and V values using the Pearson correlation coefficient to determine whether the H, S, and V parameters provided comple-

mentary or correlated information relative to standard biomechanical parameters.

Results

The computed H, S, and V channels, along with the final HSV image representing corneal dynamics, are shown in Figure 3. Examples of the final HSV images for some young and older subjects randomly selected are shown in Figure 4. There is a strong statistically significant difference in H, S, and V channels when comparing the two study groups, as Table 1 shows. The HSV analysis was based on pixel intensity tracking over time. The group mean amplitude of intensity changes was 15 (range, 13–18) for the younger group and 19 (range, 14–31) for the older group.

Table 1. Hue, Saturation, and Value Channels for Young and Older Groups and Corresponding *P* Values

	Mean ± SD		
Group	H (Hz)	S (Hz)	V (a.u.)
Young ($n = 38$)	5.3 ± 0.6	20.1 ± 1.2	2.9 ± 0.1
Older ($n = 35$)	7.2 ± 2.3	22.3 ± 3.1	3.3 ± 0.7
P	<0.001	<0.001	<0.001

a.u., arbitrary units.

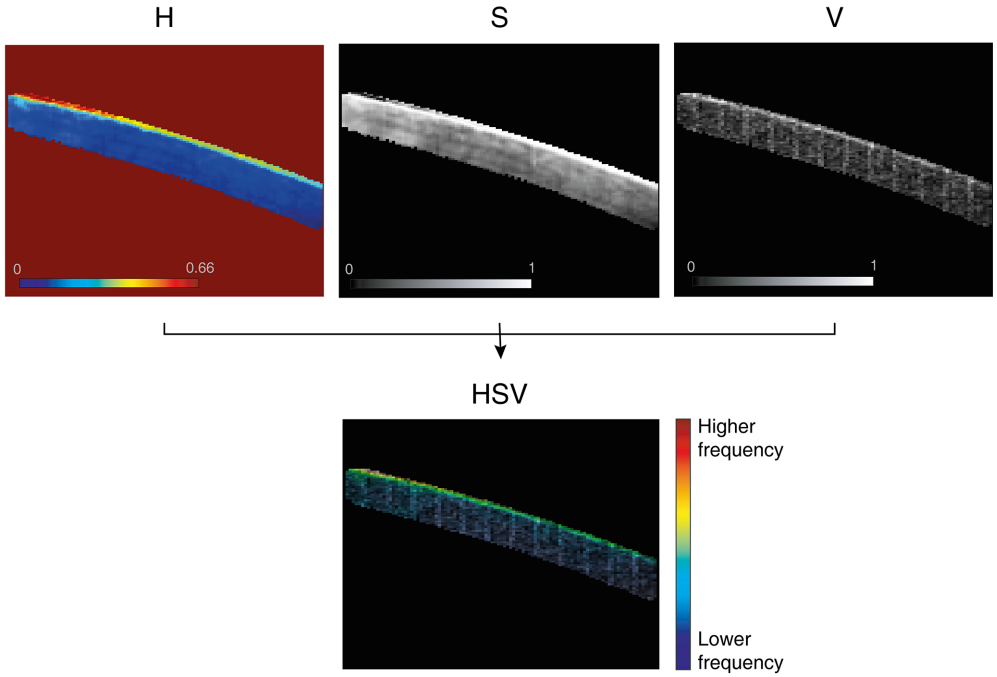

Figure 3. Representation of each individual channel (H, S, and V) obtained from pixel intensity tracking analysis, along with the final HSV image.

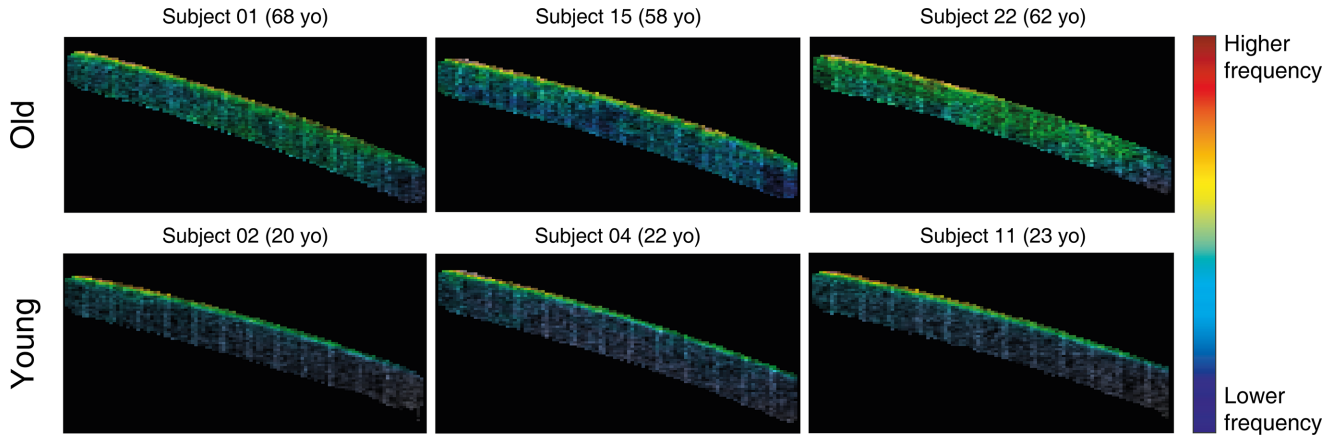

Figure 4. Examples of the resulting HSV image for different participants from the older and young groups.

Table 2. Biomechanical Parameters for Young and Older Groups

	Group, Mean ± SD		
	Young	Older	*P*
A1T (ms)	7.72 ± 0.20	7.61 ± 0.29	0.11
A1L (mm)	2.60 ± 0.41	2.38 ± 0.33	0.06
A1V (m/s)	0.18 ± 0.04	0.17 ± 0.03	0.22
A1DA (mm)	0.14 ± 0.02	0.14 ± 0.01	0.92
A1DefA (mm)	0.10 ± 0.01	0.10 ± 0.01	0.94
A1DefL (mm)	2.32 ± 0.14	2.36 ± 0.14	0.31
A1DefArea (mm^2)	0.20 ± 0.04	0.20 ± 0.04	0.93
A1dArcL (mm)	−0.019 ± 0.003	−0.020 ± 0.003	0.16
A2T (ms)	21.41 ± 1.92	20.96 ± 2.51	0.49
A2L (mm)	1.89 ± 0.50	1.79 ± 0.67	0.55
A2V (m/s)	−0.47 ± 0.18	−0.44 ± 0.17	0.57
A2DA (mm)	0.46 ± 0.09	0.55 ± 0.13	**0.01**
A2DefA (mm)	0.16 ± 0.12	0.23 ± 0.20	0.16
A2DefL (mm)	3.55 ± 0.91	4.04 ± 1.17	0.12
A2DefArea (mm^2)	0.40 ± 0.41	0.66 ± 0.79	0.15
A2dArcL (mm)	−0.03 ± 0.02	−0.05 ± 0.04	**0.04**
HCDA (mm)	1.06 ± 0.07	1.11 ± 0.08	**0.03**
PD (mm)	4.91 ± 0.27	4.86 ± 0.31	0.58
HCR (mm)	7.12 ± 0.69	6.60 ± 0.81	**0.02**

Statistically significant values ($P < 0.05$) are highlighted in bold. A1T, time from the start to A1; A1L, length of the flattened segment; A1V, velocity of corneal apex at A1; A1DA, deformation amplitude at A1; A1DefL, displacement of corneal apex from initial position to A1; A1DefL, deflection length at A1; A1DefArea, deflection area at A1; A1dArcL, change in arc length from initial state to A1; A2T, time from the start to A2; A2L, length of the flattened segment; A2V, velocity of corneal apex at A2; A2DA, deformation amplitude at A2; A2DefL, displacement of corneal apex from initial position to A2; A2DefL, deflection length at A2; A2DefArea, deflection area at A2; A2dArcL, change in arc length from initial state to A2; HCDA, distance of the corneal apex movement from initiation of the deformation to HC; PD, distance between the two surrounding peaks of the cornea at HC; HCR, central curvature radius at HC.

Table 1 shows results for the overall cornea, but the visual representation of corneal HSV images shows a distinct difference between corneal layers (Fig. 4). Specifically, the mean frequency (hue) for the epithelial layer was 9.0 ± 1.8 Hz, in contrast to the stromal layer, which exhibited a significantly lower value of 4.7 ± 2.0 Hz ($P < 0.001$, paired *t*-test).

Correcting corneal displacement induced by the air-puff stimulus is crucial to ensuring accurate pixel tracking. Our analysis revealed that older eyes exhibited a maximum displacement of 0.30 ± 0.07 mm, statistically significantly greater than the corresponding 0.23 ± 0.05 mm observed in younger eyes ($P < 0.001$, independent *t*-test).

Beyond HSV analysis, Table 2 presents the corneal biomechanical parameters extracted from the Corvis ST for both study groups. Among all of the analyzed parameters, significant differences between age groups were found in only four: A2DA, A2dArcL, HCDA, and HCR ($P < 0.05$, independent *t*-test), whereas the remaining parameters showed no statistically significant differences. Furthermore, the corneal biomechanical parameters that exhibited statistically significant differences were correlated with the H, S, and V values within each group. However, no statistically significant correlations were observed (all $P > 0.05$).

Discussion

In this study, we present a quantitative visual interpretation methodology for dynamic corneal images based on pixel intensity tracking. This method involves transitioning from the original grayscale image to a colored HSV image. It is important to note that the frequencies reported in Table 1 do not correspond to the frequency movement of the cornea. Instead,

H, S, and V are biomarkers that account for the pixel intensity change rate over time. These biomarkers are expressed in Hz, as a result of the corresponding mathematical equations, Equations 2 and 3, for its computation, but these Hz do not represent corneal vibration frequency. Instead, H, S, and V help quantify which areas of the image are more responsive to a given mechanical stimulus. Corneal responsiveness, in this context, refers to the degree to which different regions of the cornea exhibit variations in pixel intensity over time in response to an external force. Each HSV channel provides distinct yet complementary information about this response. H represents the mean frequency of pixel intensity changes over time, encoding how rapidly the intensity fluctuates and offering insight into the temporal characteristics of the corneal response. S corresponds to the spread of frequencies in the signal, where a broader frequency distribution (lower saturation) suggests more complex, less uniform motion, and higher saturation indicates a more consistent response. V represents the amplitude of pixel intensity fluctuations, capturing the extent of local corneal displacement or response to the stimulus. The HSV metric provides a spatiotemporal representation of how the cornea reacts to mechanical stimulation. As inferred in the work by Scholler et al.,[11] a reddish vibrant area of the image represents higher responsiveness to a given mechanical stimulus than a dull blue area. The specific interpretation of this concept varies depending on the dynamic image being analyzed. For example, in their work, Scholler et al.[11] associated the aspect of the HSV image with cell activity, whereas, in our case, it reflects the response to an air-puff (Figs. 3, 4).

Given the multilayered structure of the cornea, comprised of the outer epithelium and the underlying stroma, which forms about 90% of the thickness of the cornea,[19] our analysis suggests distinct biomechanical responses within these layers. A more pronounced response to movement is observed in the epithelium than in the stroma as a consequence of air-puff stimulation, as evident in Figures 3 and 4. This disparity in layer response could be a result of the lower mechanical rigidity and greater viscoelastic nature of the epithelium, which are largely dictated by its cellular composition and organization. In contrast, the stroma, primarily composed of collagen fibers and extracellular matrix, exhibits greater resistance to deformation, leading to subtler movements under mechanical stress.[19] Furthermore, the observed corneal responsiveness mechanical stimulation is not expected to be uniform across the surface of the cornea. Due to the varying intensities of the air-puff stimulus across different corneal regions, particularly influenced by the distance from the nozzle,[16] certain areas, especially those closer to the point of air-puff impact, will experience more pronounced changes. Hence, the response of the cornea to mechanical stimuli would likely be dependent not only on the depth (corneal layers) but also on the location, as already reported in previous work.[9,10,21–23]

To illustrate the potential clinical applicability of the method, we chose to compare young and older eyes because corneal tissue properties—and consequently corneal responsiveness to mechanical stimulus and corneal biomechanics—are known to be affected by age.[7] However, counterintuitively, older eyes have been shown to exhibit greater eye retraction, meaning they display more movement than younger eyes when subjected to the same air-puff mechanical stimulation.[15] In agreement with those previous results, we also found greater eye retraction in older eyes in comparison with younger eyes ($P < 0.001$, independent t-test). Prior studies have posited that this paradoxical increase in movement with age during air-puff stimulation may be associated with age-related changes in the composition of retrobulbar fat.[24]

In addition to the obtained statistically significant differences in H, S, and V channels (Table 1), the differences between younger and older eyes became markedly evident, as illustrated in Figure 4. HSV images of younger corneas presented a more uniform appearance compared to those of older individuals, highlighting the physiological changes that occur over time. HSV images of younger corneas tended to appear more uniform and cooler in tone, whereas the older corneas exhibited less homogeneity and a shift toward green–yellow hues (Fig. 4). Given that hue encodes the mean frequency of pixel intensity changes, this color shift suggests a higher dynamic response frequency in older eyes. As individuals age, their corneas experience a spectrum of morphological and biochemical changes. These alterations encompass a reduction in keratocyte density,[25] changes in collagen fiber orientation,[26] and an accumulation of advanced glycation end-products (AGEs),[27] which collectively contribute to increased tissue stiffness.[28,29] Notably, these transformations do not occur uniformly in every individual. Factors such as genetic predispositions, environmental exposures, and systemic health conditions influence the aging trajectory of the cornea, resulting in considerable interindividual variability.[30–32]

This study focused on age-related corneal changes, which are a particularly challenging case, as such subtle alterations are less detectable with current ophthalmic imaging technologies than the more pronounced changes seen in disease. In this context, the relationship

between age and corneal biomechanics remains a topic of debate, with inconsistencies reported across different studies.[33–36] Although some research has found no significant correlation between age and biomechanical parameters measured with the Corvis ST, other studies have identified age-related differences, albeit with variability in the specific parameters affected. In our study, only a few biomechanical parameters extracted from the Corvis ST showed statistically significant differences between age groups, and, even in those cases, the statistically significant P values were relatively high (0.01–0.04) (Table 2), indicating weak statistical significance. In contrast, the H, S, and V parameters demonstrated much stronger differences between groups ($P < 0.001$) (Table 1), suggesting that HSV-based analysis may be more sensitive in detecting subtle corneal tissue changes. In the current study, no statistically significant correlation was found between the H, S, and V parameters and the corneal biomechanical parameters. However, this should not be interpreted as a limitation of the methodology. Instead, it highlights that these parameters capture additional information beyond what is currently accessible through standard clinical biomechanical assessments. The absence of direct correlation suggests that the HSV-based analysis may reflect aspects of corneal behavior that are not fully described by existing clinical tools.

Achieving optimal pixel tracking is essential for the application of the proposed HSV image methodology. Our decision to track 30 out of the available 140 corneal frames was twofold: to simulate a gentler corneal stimulus than that typically provided by the Corvis ST and to mitigate potential confounding factors in pixel tracking that could skew our findings. The cornea undergoes significant transformation during air-puff stimulation, transitioning from a convex to a concave form and reverting to its original shape, all within 32.20 ms. This dynamic change is complicated by curvature change[10] and eye retraction and rotation,[9] posing substantial challenges for accurate pixel tracking. However, these complications are most pronounced during the direct air-puff impact on the cornea, specifically when it is concave—a phase we purposefully excluded from the analysis. It is important to note that, even when considering the peripheral cornea in the convex state, as we did in the current work, there is still movement indicative of corneal dynamics.[37] Among the potential artifacts cited, including retraction, rotation, and curvature changes, the latter has been shown to not significantly influence the corneal periphery in its convex state.[10] Retraction, which becomes more pronounced post-stimulus,[9,14] can be efficiently corrected through registration using the anterior corneal border as a reference, as was done in the present work. As for rotation, a study by Boszczyk et al.[9] indicated a tendency for the eye globe to rotate nasally during measurements, albeit predominantly while the cornea is concave. This suggests that rotation might not interfere significantly if analyses are confined to phases when the cornea is convex. Nonetheless, additional validation to confirm these inferences would be advisable.

In the current work, HSV analysis was not intended to directly assess corneal biomechanics per se. Instead, we introduced a methodology specifically designed to visually identify areas most responsive to a mechanical stimulus. The presented image processing method is preliminary but holds promise for broader clinical applications. One particularly relevant application lies in managing keratoconus, a condition known for localized alterations in corneal tissue and biomechanical properties. A preliminary internal analysis conducted on a small cohort of 10 clinical keratoconus eyes revealed statistically significant differences in all three HSV parameters when compared to the young group ($P < 0.001$). This suggests the potential of the method to detect corneal tissue changes associated with the disease, although further studies with larger sample sizes are needed to fully explore its clinical utility. Utilizing the HSV methodology could significantly enhance the precision in delineating the keratoconus cone, a critical step in tailoring individualized management plans for patients. Beyond keratoconus, this approach has the versatility for deployment in a spectrum of other corneal conditions that manifest alterations in tissue characteristics.

Similarly, the HSV analysis conducted here using clinically available images could be adapted to other imaging technologies. The research community is increasingly interested in exploring corneal vibrations using alternative imaging modalities, such as optical coherence tomography (OCT),[17] while also seeking gentler methods of mechanical stimulation on the cornea. In this context, optical coherence elastography (OCE) emerges as a pivotal technology.[38] OCE extends OCT capabilities, facilitating the non-invasive assessment of the biomechanical responses of the cornea by mapping elasticity contrasts within the tissue. Utilizing low-frequency vibrational stimuli, it conducts these assessments under milder, controlled conditions, thereby enhancing patient comfort and reducing potential artifacts and variability.[39–42] This emerging approach to studying corneal responses, yet restricted to laboratory prototypes, underscores the necessity for innovative methodologies capable of

extracting meaningful insights from corneal dynamics data, particularly in scenarios where corneal deformation is significantly subtler than that produced by standard air-puff stimulation. Hence, the HSV analysis technique used in our study with clinically available images could be adapted for use in OCE. Implementing the HSV method within OCE studies could provide advantages not currently available from clinical equipment. This includes the ability to observe corneal responses over longer periods, yielding a richer collection of temporal data, alongside more precise control over the mechanical stimulus. However, it is important to note that the corneal excitation used in our study is significantly more pronounced than that typically used in OCE. There is no existing evidence to suggest that pixel intensity changes during OCE, thus raising questions about the sensitivity and applicability of the HSV method in such a context. Additionally, using the proposed HSV method, details about corneal vibrations, such as the direction of their propagation, are not captured, leading to a loss of potentially valuable information. Despite this, the potential of integrating HSV analysis into OCE warrants investigation, as it could offer a novel perspective in understanding subtle corneal biomechanics and further enhance the diagnostic capabilities of OCE.

This study has several limitations that should be considered when interpreting the results. First, the HSV analysis was performed on a limited number of frames (30 out of 140), focusing on the recovery phase after the air puff to minimize artifacts caused by curvature changes and eye retraction. Whereas this enhances the reliability of pixel tracking, it restricts the temporal resolution and may overlook some aspects of corneal deformation. Second, the methodology was applied to the peripheral cornea rather than the central region, which may limit direct comparisons with conventional biomechanical parameters typically derived from the central cornea. Third, although statistically significant differences were found between age groups, the visual distinctions in HSV images are sometimes subtle and may not be easily perceptible without quantitative analysis. Finally, although the method shows potential for broader clinical applications, it has only been validated on a healthy population; its utility in pathological conditions, such as keratoconus, requires further investigation on larger clinical datasets.

In conclusion, although further validation is necessary to determine the clinical impact of the presented methodology, it marks a significant step forward in corneal dynamics analysis using clinically available images. Given that the Corvis ST remains the only clinically available device for in vivo corneal biomechanics, integrating HSV analysis as a complementary tool could provide an enhanced understanding of corneal response dynamics. Utilizing the HSV color space to interpret corneal dynamics through spectral analysis of pixel intensity tracking facilitates a quantitative visual interpretation of the response of the cornea to mechanical stimuli.

Acknowledgments

Supported by a grant (TED2021-130723A-I00) funded by the Spanish Ministry of Science and Innovation (MCIN/AEI/10.13039/501100011033), the European Union NextGenerationEU/PRTR, and the European Research Council under the European Union's Horizon Europe Research and Innovation Programme (101162733).

Disclosure: **A.R. Arizcuren**, None; **A. Consejo**, None

References

1. Piñero DP, Alcón N. Corneal biomechanics: a review. *Clin Exp Optom*. 2015;98(2):107–116.
2. Chong J, Dupps WJ, Jr. Corneal biomechanics: measurement and structural correlations. *Exp Eye Res*. 2021;205:108508.
3. Esporcatte LP, Salomão MQ, Lopes BT, et al. Biomechanical diagnostics of the cornea. *Eye Vis (Lond)*. 2020;7(1):9.
4. Consejo A, Solarski J, Karnowski K, Rozema JJ, Wojtkowski M, Iskander DR. Keratoconus detection based on a single Scheimpflug image. *Transl Vis Sci Technol*. 2020;9(7):36.
5. Issarti I, Consejo A, Jiménez-García M, Kreps EO, Koppen C, Rozema JJ. Logistic index for keratoconus detection and severity scoring (Logik). *Comput Biol Med*. 2020;122:103809.
6. Blackburn BJ, Jenkins MW, Rollins AM, Dupps WJ. A review of structural and biomechanical changes in the cornea in aging, disease, and photochemical crosslinking. *Front Bioeng Biotechnol*. 2019;7:66.
7. Elsheikh A, Wang D, Brown M, Rama P, Campanelli M, Pye D. Assessment of corneal biomechanical properties and their variation with age. *Current eye research*. 2007;32(1):11–19.
8. Blackburn BJ, Jenkins MW, Rollins AM, Dupps WJ. A review of structural and biomechanical changes in the cornea in aging, disease, and photochemical crosslinking. *Front Bioeng Biotechnol*. 2019;7:66.

9. Boszczyk A, Kasprzak H, Jóźwik A. Eye retraction and rotation during Corvis ST 'air puff' intraocular pressure measurement and its quantitative analysis. *Ophthalmic Physiol Opt*. 2017;37(3):253–262.
10. Kasprzak H, Boszczyk A. Numerical analysis of corneal curvature dynamics based on Corvis tonometer images. *J Biophotonics*. 2016;9(5):436–444.
11. Scholler J, Groux K, Goureau O, et al. Dynamic full-field optical coherence tomography: 3D live-imaging of retinal organoids. *Light Sci Appl*. 2020;9(1):140.
12. Miażdżyk M, Consejo A, Iskander DR. Assessing and compensating for the confounding factors in Scheimpflug-based corneal densitometry. *Biomed Opt Express*. 2022;13(12):6258–6272.
13. Consejo A, Alonso-Caneiro D, Wojtkowski M, Vincent SJ. Corneal tissue properties following scleral lens wear using Scheimpflug imaging. *Ophthalmic Physiol Opt*. 2020;40(5):595–606.
14. Vinciguerra R, Elsheikh A, Roberts CJ, et al. Influence of pachymetry and intraocular pressure on dynamic corneal response parameters in healthy patients. *J Refract Surg*. 2016;32(8):550–561.
15. Simonini I, Pandolfi A. The influence of intraocular pressure and air jet pressure on corneal contactless tonometry tests. *J Mech Behav Biomed Mater*. 2016;58:75–89.
16. Eliasy A, Chen KJ, Vinciguerra R, et al. Determination of corneal biomechanical behavior *in-vivo* for healthy eyes using Corvis ST tonometry: stress-strain index. *Front Bioeng Biotechnol*. 2019;7:105.
17. Curatolo A, Birkenfeld JS, Martinez-Enriquez E, et al. Multi-meridian corneal imaging of air-puff induced deformation for improved detection of biomechanical abnormalities. *Biomed Opt Express*. 2020;11(11):6337–6355.
18. Othman MK, Abdulla AA. Enhanced single image dehazing technique based on HSV color space. *UHD J Sci Technol*. 2022;6(2):135–146.
19. Espana EM, Birk DE. Composition, structure and function of the corneal stroma. *Exp Eye Res*. 2020;198:108137.
20. Koprowski R, Wilczyński S. Corneal vibrations during intraocular pressure measurement with an air-puff method. *J Healthc Eng*. 2018;2018:5705749.
21. Boszczyk A, Kasprzak H, Siedlecki D. Non-contact tonometry using Corvis ST: analysis of corneal vibrations and their relation with intraocular pressure. *J Opt Soc Am A Opt Image Sci Vis*. 2019;36(4):B28–B34.
22. Boszczyk A, Kasprzak H, Przeździecka-Dołyk J. Novel method of measuring corneal viscoelasticity using the Corvis ST tonometer. *J Clin Med*. 2022;11(1):261.
23. Koprowski R, Ambrósio R, Jr. Quantitative assessment of corneal vibrations during intraocular pressure measurement with the air-puff method in patients with keratoconus. *Comput Biol Med*. 2015;66:170–178.
24. Regensburg NI, Wiersinga WM, van Velthoven ME, et al. Age and gender-specific reference values of orbital fat and muscle volumes in Caucasians. *Br J Ophthalmol*. 2011;95(12):1660–1663.
25. Gambato C, Longhin E, Catania AG, Lazzarini D, Parrozzani R, Midena E. Aging and corneal layers: an in vivo corneal confocal microscopy study. *Graefes Arch Clin Exp Ophthalmol*. 2015;253:267–275.
26. Gogola A, Jan NJ, Brazile B, et al. Spatial patterns and age-related changes of the collagen crimp in the human cornea and sclera. *Invest Ophthalmol Vis Sci*. 2018;59(7):2987–2998
27. Kandarakis SA, Piperi C, Topouzis F, Papavassiliou AG. Emerging role of advanced glycation-end products (AGEs) in the pathobiology of eye diseases. *Prog Retin Eye Res*. 2014;42:85–102.
28. Liu J, Roberts CJ. Influence of corneal biomechanical properties on intraocular pressure measurement: quantitative analysis. *J Cataract Refract Surg*. 2005;31(1):146–155.
29. Meek KM, Boote C. The organization of collagen in the corneal stroma. *Exp Eye Res*. 2004;78(3):503–512.
30. Galor A, Britten-Jones AC, Feng Y, et al. TFOS lifestyle: impact of lifestyle challenges on the ocular surface. *Ocul Surf*. 2023;28:262–303.
31. Markoulli M, Ahmad S, Arcot J, et al. TFOS Lifestyle: impact of nutrition on the ocular surface. *Ocul Surf*. 2023;29:226–271.
32. Vithana EN, Aung T, Khor CC, et al. Collagen-related genes influence the glaucoma risk factor, central corneal thickness. *Hum Mol Genet*. 2011;20(4):649–658.
33. Elsheikh A, Geraghty B, Alhasso D, et al. In vivo corneal biomechanical properties with corneal visualization Scheimpflug technology in Chinese population. *J Ophthalmol*. 2016;2016:7840284.
34. Lee H, Kang DSY, Ha BJ, et al. Biomechanical properties of the cornea using a dynamic Scheimpflug analyzer in healthy eyes. *Yonsei Med J*. 2018;59(9):1115–1122.
35. Kamiya K, Shimizu K, Ohmoto F. Effect of aging on corneal biomechanical parameters using the ocular response analyzer. *J Refract Surg*. 2009;25:888–893.

36. Wang W, He M, He H, Zhang C, Jin H, Zhong X. Corneal biomechanical metrics of healthy Chinese adults using Corvis ST. *Cont Lens Anterior Eye*. 2017;40(2):97–103.
37. Redaelli E, Grasa J, Calvo B, Rodriguez Matas JF, Luraghi G. A detailed methodology to model the non contact tonometry: a fluid structure interaction study. *Front Bioeng Biotechnol*. 2022;10:981665.
38. Akca BI, Chang EW, Kling S, et al. Observation of sound-induced corneal vibrational modes by optical coherence tomography. *Biomed Opt Express*. 2015;6(9):3313–3319.
39. Larin KV, Sampson DD. Optical coherence elastography–OCT at work in tissue biomechanics. *Biomed Opt Express*. 2017;8(2):1172–1202.
40. Wang S, Larin KV. Optical coherence elastography for tissue characterization: a review. *J Biophotonics*. 2015;8(4):279–302.
41. Ramier A, Eltony AM, Chen Y, et al. In vivo measurement of shear modulus of the human cornea using optical coherence elastography. *Sci Rep*. 2020;10(1):17366
42. McAuley R, Nolan A, Curatolo A, et al. Co-axial acoustic-based optical coherence vibrometry probe for the quantification of resonance frequency modes in ocular tissue. *Sci Rep*. 2022;12(1):18834.